AD-785 607

HYPERVELOCITY IMPACT SHOCK-INDUCED
DAMAGE TO STEEL ARMOR

John W. Bond, Jr.

Army Mobility Equipment Research and
Development Center
Fort Belvoir, Virginia

1973

BOND

D D C
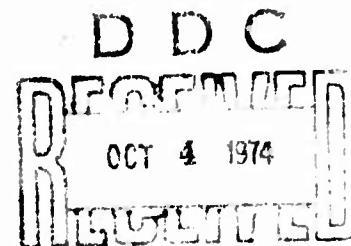
OCT 4 1974

HYPERVELOCITY IMPACT SHOCK-INDUCED
DAMAGE TO STEEL ARMOR

JOHN W. BOND, JR., DR.
MOBILITY EQUIPMENT RESEARCH AND DEVELOPMENT CENTER
FORT BELVOIR, VIRGINIA

1. INTRODUCTION

An In-house Laboratory Independent Research (ILIR) program
has been conducted at MERDC to design hypervelocity projectiles
that maximize back-face spallation in steel armor. The pro-
jectiles are small (.5 to 5 gm each) so that several hundred of
them can be located on one end of an explosive driver weighing 15
to 30 kg. The projectiles would be ejected in a near-vertical
downward direction toward a target in a shotgun pattern at eject
velocities of 8-10 km/sec and at a stand-off distance of 20 to 50
meters. This enables large lethal, or damage radii, of the order
of tens of meters, to be considered. The primary target for the
experimental program has been steel armor 2 to 5 cm thick.
Damage would be by back-face spallation and fragmentation and
resultant effects on soft interior components (of military vehicles)
such as cabling, munitions, fuel, equipment, instruments, and
personnel.

When the program started two years ago there was
insufficient information on spallation physics to design the type of
projectile desired. Accordingly, a program was started to obtain
the needed experimental and analytical information. The specific
goal was to design a projectile capable of shaping the pulse
induced in the steel target in such a way that a large amount of
steel was ejected from the back-face of the specimen in the form

97

BOND

of many small damaging fragments. During the course of the
research, new phenomena were observed which are reported herein.
In particular, the importance of the 130-kbar phase change in
martensitic steel and its effect on spallation is discussed.

Over 100 successful impact experiments were performed in
the Naval Research Laboratory (NRL) light gas gun facility. The
experiments were designed and the results analyzed at MERDC.
Metallurgical examination of the impacted specimens was done at
the Stanford Research Institute (SRI), with some assistance from
Sandia Laboratories Albuquerque (SLA). Mechanical material prop-
erties of the target materials were measured at MERDC.

In order to develop reliable theory and associated analyt-
ical tools, simple spherical projectiles, most weighing less than
1 gm, were used. Impact angles were generally normal, although
a few non-normal impacts were made. A few impacts were made
with both simple and composite non-spherical projectiles. Pro-
jectile materials included nylon, lexan, water, heavy oil, steel,
MgLi, and several different ceramics

The reasoning behind these choices of projectile materials
was rather complicated. It was based on the fact that the proposed
warhead is weight limited rather than volume limited. This en-
ables more projectiles of the same size to be carried, or else
larger projectiles may be used. Size is important because the pro-
jectile diameter should be of the order of, or greater than the
target thickness in order to optimize spall. There is some experi-
mental evidence that much smaller (non-penetrating) projectiles
are efficient spallators (3). (A spallator is a projectile that
optimizes back-face spall. A penetrator optimizes penetration.)
Finally, the vaporization or sublimation energy of the projectile
material should be small compared to the kinetic energy of impact.
The general idea is to convert most of the impact energy into
induced shock. This means that inefficient processes such as
penetration should be minimized.

Most of the targets were wrought, homogeneous steel plate
stock 1. 25 cm and 2. 5 cm thick. The steel was a carbon

BOND

manganese-nickel-chromium-molybdenum alloy which was
austenitized at 900°C, water quenched, and tempered at 540°C.
The representative hardness was 360 Brinnel (Bhn), and the
approximate quasi-static tensile strength was 12 kbars. The
dynamic spall strength corresponded to a critical tensile pressure
of 38 kbars (1, 2, 3, 4).

After impact, the target specimens were dissected through
the crater center, polished, etched, and examined metallurgically.
Extensive 2-d code calculations of the impact spall phenomena were
made by SLA for one specimen.

In Section 2, below, the experimental results are
summarized. They are analyzed and discussed in Section 3. The
2-d computations performed by SLA are described in Section 4.
The 130-kbar phase change and spall phenomena are discussed in
the remaining sections.

2. EXPERIMENTAL RESULTS

Photographs of dissected impact craters are shown in
Figure 1. The target material for Fig. 1a was 1.25 cm thick
wrought steel. The projectile was a 0.52 gm nylon sphere with a
diameter of 0.95 cm and an impact velocity of 5.18 km/sec. The
crater is representative of craters formed by impact of lexan-
encased H_2O and solid nylon spheres The walls of such craters
exhibit a series of evenly spaced ridges, or serrations, which are
symmetric about a central axis of rotation. The macrocracks ob-
served extend downwards from the bottom of the valleys in the crater
floor. In Fig. 1b the target was 2.53 cm wrought steel and the pro-
jectile was a 0.7 gm steel sphere. In the case of steel-on-steel im-
pacts the serrations in the craters are not observed and the macro-
cracks extend upwards. (This difference has not been explained.)
In Figure 2 is shown a 10X photograph of the bottom of the center of
a crater produced by a 6.03 km/sec impact of a 0.35 gm H_2O/lexan
sphere on a 2.5 cm wrought steel target. The (apparent) shaded
region extends completely around the crater. This region is readily
visible on almost all impact specimens. It has extremely high
hardness (500 Bhn) and displays a very fine untempered,
martensitic microstructure. This observed metallurgical
transformation has been shown to be due to the 130-kbar poly-

99

BOND

morphic phase transition in iron or martensitic steel (3, 4). The fine adiabatic shear lines are readily observable on this photograph. Also, note the large voids below the bottom of the crater.

When the stress wave, induced at impact, travels through the target and reflects in tension from the back-face, a spall layer, or gap, is produced as seen in Figure 1. Spall is not observed for these conditions at velocities below about 3 km/sec. At slightly greater velocities incipient spall is observed by the appearance of microcracks. The microcracks coalesce to form a complete spall layer at about 3.1 km/sec. As the impact velocity is increased the width and diameter of the spall layer also increases, and at some higher velocity the back-face plugs or fragments. Non-adiabatic shear occurs at the outer edge of the spall layer. For a 0.52 gm nylon sphere on 1.25 cm wrought steel, back-face plugging occurs at about 5.8 km/sec. For smaller (lighter) spheres, or for thicker targets, the plugging (or back-face fragmenting) velocity is higher.

In spite of the extensive experimentation described above (as well as all other experimentation performed in the US) it is still not possible to design an effective spallator. However, a few preliminary guidelines have been outlined. Briefly, it is clear that pulse shaping is the key to the production of damaging back-face spall. This is exemplified in Figure 3 which shows the reflection and resultant spall of a triangular stress pulse. The incident pulse reflects in tension at the free surface x_O. Upon exceeding the spall threshold, a spall layer is formed at x_1. The distance x_1-x_O must be sufficiently small so that the back-face can be spalled and fragmented, but sufficiently large so that a damaging amount of back-face material is ejected.

After the spall layer is formed at x_1, the subsequent stress pulse reflects at x_i rather than at x_O. This can result in the formation of a second spall layer at x_2. Obviously this sequence of events can be repeated to form multiple spall layers. In order to prove this hypothesis several different projectile configurations were tested. One of these configurations was a hollow plastic sphere. The reasoning here was that upon impact

BOND

more mass would be delivered at the impact periphery and "double-impact" conditions for thin flyers would exist at the impact center. This heuristic prediction was eminently borne out in several experiments in which the projectiles were hollow spheres. An example is shown in Figure 4. In this case the projectile was a hollow lexan sphere weighing 0.56 gm with a diameter of 1.08 cm and an impact velocity of 5.59 km/sec. Note the double spall layer and the back-face fragmentation.

A few other impact experiments were performed in which the projectile was computer designed to optimize back-face spall. These experiments were particularly successful in showing that back-face spall can be optimized.

3. DISCUSSION OF EXPERIMENTAL RESULTS

In general a well-conceived experimental program produces results that have not been predicted theoretically. This program is no exception. The experimental "surprises" are too numerous to cover in this report; but a few of the more important results can be discussed. These are listed below:

a. Serrations are formed at the crater floor for nylon-and water-steel impacts. These have not been explained; in particular, the reason for the serration formation on nylon-steel impact and the lack of serration formation on steel- steel impact has not been explained.

b. Preliminary or tentative explanation of the macrocracks observed for nylon-steel impacts has been given. However, this explanation fails to show why the macrocracks extend upwards for steel-steel impacts as compared to downwards for nylon-on-steel impacts.

c. Adiabatic shear lines are observed below the crater floor in almost all cases. However, their role in the damage process has not been explained.

e. The importance of the observed 130-kbar phase change has been explained for one case. This is discussed in the next

BOND

section. Much more work is needed on this phenomenon.

f. Spallation. The 2-d computer calculations performed by SLA have shown excellent agreement with one impact experiment. This applies to the configuration and location of the spall layer for a relatively simple case. If this work could be extended to more important and relevant cases it would be of extreme significance.

g. General Summary

(1) Metallographic/Fractographic Features

As indicated previously considerable circumstantial evidence leads to the conclusion that the dark-etching hemispherical volume of material under the impact site, such as shown in Fig. 2, has undergone the pressure-induced phase transformation:

$$\alpha \rightleftharpoons \epsilon$$

Material within this zone is of significantly finer grain structure and higher hardness than material elsewhere. Back surface laser interferometer records obtained by SLA in plate slap experiments exhibit clearly the disturbance attributable to a wave reflected from a denser phase (4).

Profuse shear bonding was observed in the subcrater region and is felt to play an important role in the cratering process. The long cracks extending into the armor steel from the crater walls tend to lie on shear bands and tend to join up to isolate pieces of material that form part of the ejecta.

Shear bands that are not associated with the crater walls are also prominent in the transformed region. A number of equiaxed microfractures having a ductile appearance are generally present in this region, linked together by adiabatic shear bands, which are easily observable because of their distinct etching behavior. Again, cracks are observed to have formed in the bands, and suggest the mechanism of material removal in this region. No evidence of adiabatic shear was found in the back surface regions.

BOND

Fracture damage in the back surface region proceeds by the nucleation, growth, and coalescence of microfractures, followed by a widening of the resulting macrocrack and subsequent scabbing of the back surface by a shearing process that does not appear to be adiabatic. Observations of back surface damage at all stages of development were possible because of the wide variations in impact conditions. However, detailed stress histories were not obtained.

(2) Correlations with Stress History

An attempt was made to correlate metallographic and fractographic features observed in the specimens with stress histories. This is described in the next section of this report. However, many of the essential features of the stress history may be similar in other experiments. Thus the correlations may be common to hypervelocity impact in general, although many more experiments, metallurgical analysis, and theoretical extensions are needed before this statement can be properly delineatized. The observed features for the single case described above were predicted (post-test) with outstanding accuracy by the SLA.

4. 2-D COMPUTATIONS

It was fortuitous that the MERDC impact spallation experiments began about one year before SLA scheduled for usage their new two-dimensional hydrodynamic codes. Accordingly, in May 1973, SLA began to code the impact of a nylon sphere on to 1.25 cm steel armor. The experimental results are shown in Figure 1. The impact velocity was 5.18 km/sec and the projectile mass 0.52 gm. The results of the SLA effort are described below (4).

Two-dimensional code calculations of the above test were performed at SLA using both the CSQ Eulerian Code and the TOODY Langrangian code with rezoning. The initial impact pressure was about 400 kbar which causes iron and martensitic steel near the impact point to undergo the $\alpha \rightarrow \epsilon$ polymorphic phase change. The nylon sphere greatly distorts and goes into a liquid-partially vapor state. The steel plate suffers a large distortion near the impact point and requires both an accurate elastic-plastic model and a good material failure model elsewhere in the plate. Also, a high degree of resolution is

BOND

required for predicting complete or internal spallation because of the attenuation of the initial compressive pulse, its reflection, and the interaction of the compressive and the reflected release wave must all be calculated accurately.

The 130-kbar phase change, the correct spall strength, and an adequate failure model have all been determined to be very important for predictive and interpretive calculations. A detailed examination of the stress histories for the cases with and without the phase change has shown why different failures should be expected in these two cases (4). When the phase change is included in the calculations, the loading portion of the stress wave consists of two parts as the wave separates at 130 kbar. More important is the difference observed as unloading occurs; a rarefaction shock is present when the phase change is included. These differences in the stress wave structure not only cause a cylindrical-conical failure to occur directly below the crater, but also result in a propagating pulse that is nearly square for the case with a phase change and nearly triangular without. The square pulse, upon reflection from a free surface, transfers essentially all the momentum to the spall layer, whereas the triangular pulse is not nearly as effective in momentum transfer. This clearly shows the importance of the stress pulse shape in producing effective spall.

The measured spall stress of 38 kbar (2, 4) for the MS 12560 steel was used in the above calculations, and the results showed excellent agreement with the experiment. This was especially true for the Lagrangian results where the crater diameter, crater depth, spall layer thickness, spall length, spall bulge, cylindrical-conical failure, and the area that undergoes a phase change all show nearly one-to-one correspondence with experiment. The calculation did not, however, reproduce the serrations in the crater floor, nor the macrocracks and adiabatic shear observed below the crater floor.

When the phase change is included in both the CSQ and the TOODY calculations, the only significant difference is the spall length (or diameter). This difference is a direct result of the material failure treatment at the spall plane where a material coordinate treatment allows a higher accuracy. The very good numerical and experimental agreement demonstrates the capability of the codes to solve a wide class of difficult and important problems although

much more correlation between calculations and experiments is
needed.

5. THE 130-KBAR PHASE CHANGE IN MARTENSITIC STEEL

In recent years a number of measurements have been made of
the high pressure properties of iron in the region of the $\alpha \rightarrow \epsilon$ phase
transition. These indicate that at room temperature the transition
occurs in the region of 130 kbars and that it is abaric, initiating at
about 130 kbars and going to completion at pressures greater than
170 kbars. The observed specific volume change associated with the
transition is $\Delta v \approx .0066$ cm^3/gm and the compression ratio at the
onset of the transition is $X \approx .943$. Here x is the specific volume, v,
divided by the specific volume, v_o, of α-Fe at 0°K and zero pressure(6).

The phase diagram of Fe is shown in Figure 5. According to
the SLA calculations the shock temperature in the Fe does not go
sufficiently high to drive the steel into the γ phase. However, the
shock pressure does get sufficiently high to drive the steel into the
phase from which it reverts, on cooling, to the α phase, with a con-
sequent change in grain structure and other mechanical properties.
Direct active measurements to show this change have not been made
but a combination of theory, computations, and metallurgical analysis
indicates that the above history is correct

6. COMPLETE AND BACKFACE SPALL
Microcracks and voids begin to form when the tensile stress
reaches the "spall threshold" or the incipient spall strength. For
practical purposes a certain microcrack size or density is assigned to
this value.

As the tensile stress exceeds the spall threshold the micro-
cracks begin to coalesce until a complete spall layer is formed. For
the impact experiments with spherical projectiles described in this
paper, the spall layer is generally parallel to the backface of the tar-
gets with its center line at a distance (d) from the backface. For a
given type of projectile d is constant over the velocity range from 3 to
7 km/sec. The spall layer has a thickness δ (perpendicular to the back-
face), which increases rapidly with velocity above the incipient thresh-
old. In addition to the spall layer thickness there is a backface bulge
with height (h), which is equal to δ. As long as the spall layer is formed
near the backface h is a useful experimental (or empirical) parameter since

BOND

It can be measured with good accuracy, whereas measurements of δ are sometimes ambiguous. The spall layer has a diameter D (parallel to the backface) that increases slightly with impact velocity. It grows to be somewhat greater than the crater diameter (parallel to and at the target surface). At some high impact velocity the backface "plugs" or fragments, i.e., material of thickness d and (approximate) diameter D is ejected from the backface either as a single plug, or as a number of small fragments. The impact velocity to produce incipient spall is V_0 and for backface spall it is V_{∞}. As will be seen V_{∞} appears to be about twice V_0 for the experiments described.

Backface bulge height h is plotted on linear paper as a function of impact velocity for three different cases in Figure 7. It is seen that the experimental points lie reasonably well on smooth curves. The points have been plotted for the .52-gm nylon sphere on the 1.25-cm steel target on semi-log paper in Figure 8. They fall well on a straight line which suggests that the fractional increase in h (or δ) increases with incremental velocity, i.e.,

$$\Delta h = h \, k \, \delta \Delta V$$

where k is a constant. Upon integration this becomes

$$h = h_0 \, exp \, k \, (V - V_0)$$

For the purposes here h_0 can be assumed to correspond to the bulge height at incipient spall, with V_0 the corresponding impact velocity.

REFERENCES

1. Two-Dimensional Spallation Induced by Hypervelocity Impact in Wrought Steel Plate, J.W. Bond, and G.W. Ullrich, MERDC report 2067, July 1973 (U)

2. Personal Communication, A. Stevens, SLA, 1973 (U)

3. Support of Armor Fragmentation Studies, D.A. Shockey, SRI Project PYU 2151, 16 Oct 1973 (U)

4. Hypervelocity Impact and Associated Phenomena, D.A. Shockey, SRI Project PYU 2151, 19 Dec 1973 (C)

5. Metallurgical Effects at High Strain Rates, D.J. Pastine, Plenum Press 1973.

6. Equation of State of the Alpha and Epsilon Phases of Iron, D.J. Andrews, Washington State University, WSU SDL 70-05, Nov 1970.

7. Dynamic Mechanical Behavior or Iron, D.R. Curran in Shock Waves and the Mechanical Properties of Solids, ed J.J. Burke and V. Weiss, Syracuse Union Press, 1971.
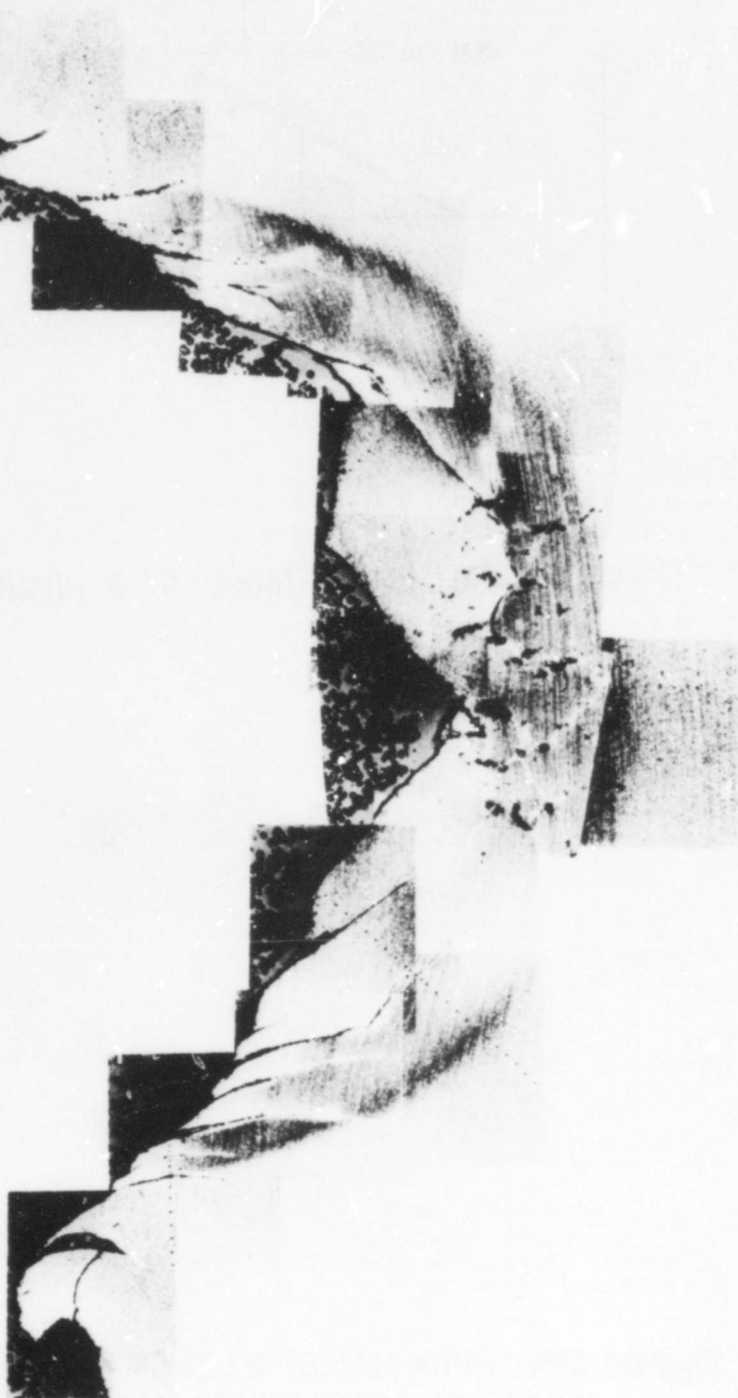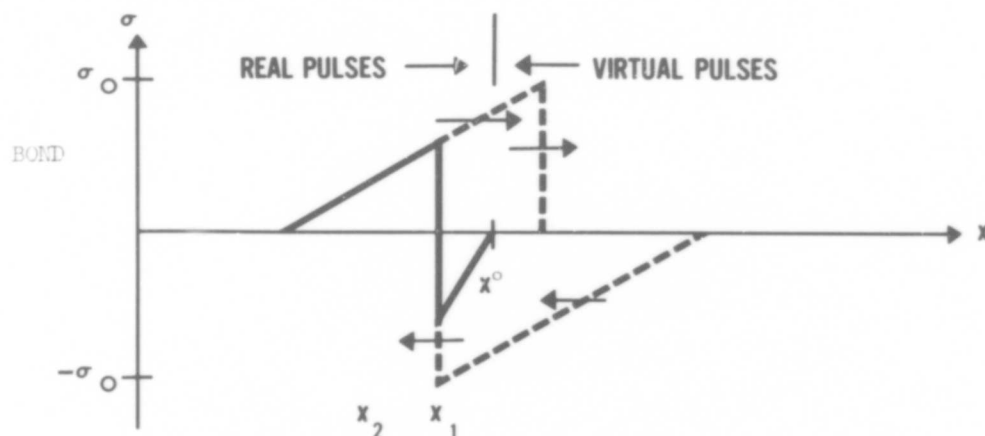
Figure 3. SPALL LAYER FORMED BY A TRIANGULAR PULSE

Figure 4. SPALLATION DAMAGE IN 1.25-CM WROUGHT STEEL
BY HOLLOW LEXAN SPHERE. MASS=.565 GM,
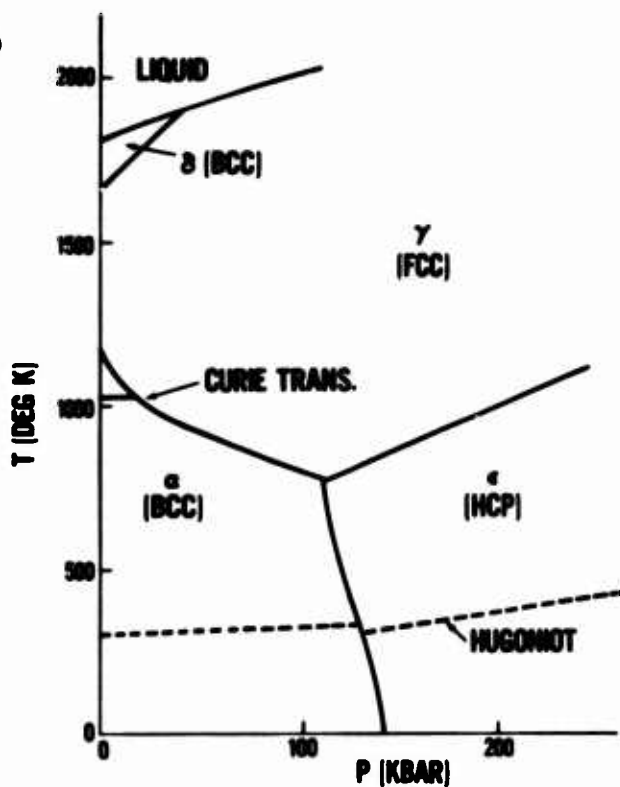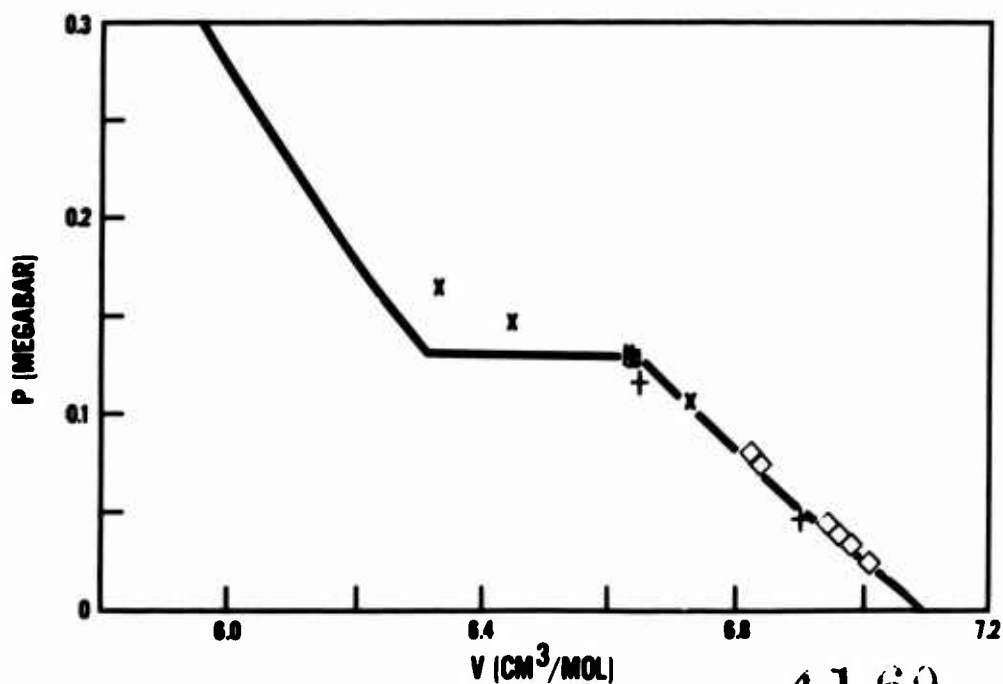DIAM=1.08 GM, IMPACT VELOCITY=5.6 KM/SEC

Figure 5. PHASE DIAGRAM OF IRON
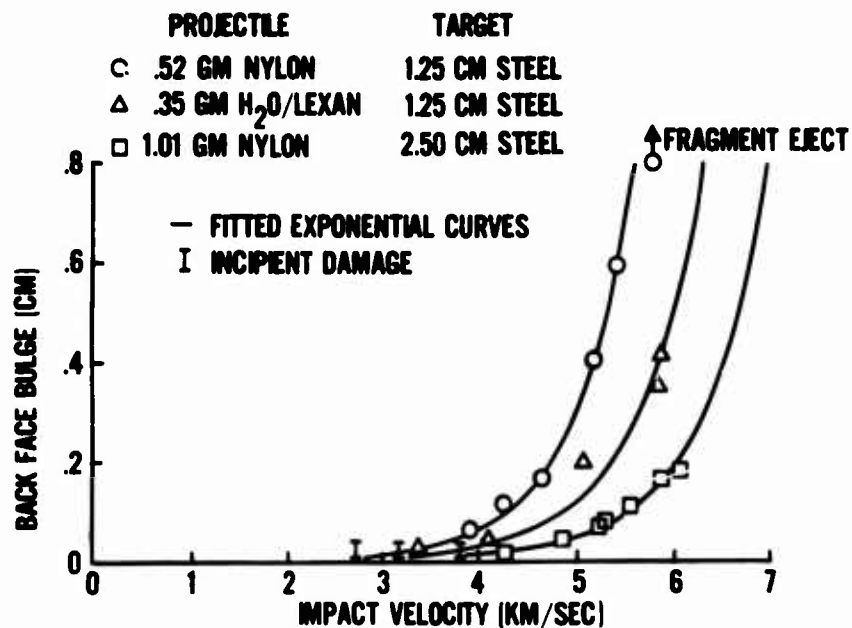

4169

Figure 6. HUGONIOT STATES OF IRON
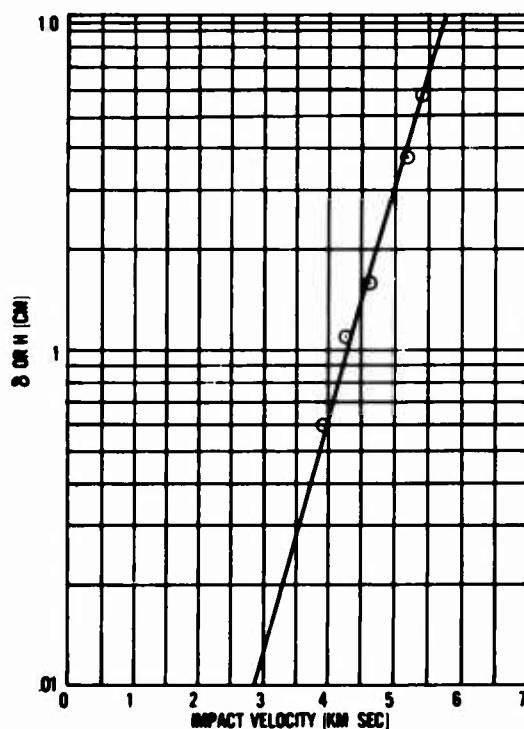
Figure 7. SPALL DAMAGE IN HOMOGENEOUS
WROUGHT STEEL PLATE

Figure 8. BACKFACE BULGE (OR SPALL LAYER
THICKNESS) VS IMPACT VELOCITY